Chemistry & Biology, Vol. 9, 639–645, May, 2002, ©2002 Elsevier Science Ltd. All rights reserved. PII S1074-5521(02)00138-2

Crystal Structure of a Squalene Cyclase in Complex with the Potential Anticholesteremic Drug Ro48-8071

Alexander Lenhart, Wilhelm A. Weihofen, Axel E.W. Pleschke, and Georg E. Schulz[1]
Institut für Organische Chemie und Biochemie
Albert-Ludwigs-Universität
D-79104-Freiburg im Breisgau
Germany

Summary

Squalene-hopene cyclase (SHC) catalyzes the conversion of squalene into pentacyclic compounds. It is the prokaryotic counterpart of the eukaryotic oxidosqualene cyclase (OSC) that catalyzes the steroid scaffold formation. Because of clear sequence homology, SHC can serve as a model for OSC, which is an attractive target for anticholesteremic drugs. We have established the crystal structure of SHC complexed with Ro48-8071, a potent inhibitor of OSC and therefore of cholesterol biosynthesis. Ro48-8071 is bound in the active-center cavity of SHC and extends into the channel that connects the cavity with the membrane. The binding site of Ro48-8071 is largely identical with the expected site of squalene; it differs from a previous model based on photoaffinity labeling. The knowledge of the inhibitor binding mode in SHC is likely to help develop more potent inhibitors for OSC.

Introduction

Oxidosqualene cyclase (OSC) catalyzes the key step in the conversion of the linear triterpene (3S)-2,3-oxidosqualene into fused-ring compounds such as cycloartenol in plants or lanosterol in mammals and fungi [1, 2]. Lanosterol is the precursor of cholesterol and numerous steroidal hormones. The prokaryotic counterpart of this enzyme is squalene-hopene cyclase (SHC), which transforms squalene into the five-membered ring systems hopene and diplopterol (Figure 1). These compounds are processed to a great variety of hopanoids stabilizing the bacterial membrane [3]. Both OSC and SHC are membrane proteins, as demonstrated by solubilization experiments with detergents. The sequence identity within the individual prokaryotic and eukaryotic families is always above 31%. The sequence identity between these two families ranges from 16% to 21%. The sequences of human OSC and that of the only structurally known SHC from *A. acidocaldarius* [4] contain 20% identical residues at important positions and are therefore clearly homologous.

The structure of SHC was solved in three crystal forms [4, 5] showing a dimeric monotopic integral membrane protein consisting of two α/α barrel domains. A large central cavity is enclosed by loops and a short five-stranded β sheet linking the barrel domains. Asp376 of the conserved motif DXDD is located at the "top" of the cavity, where it initiates the cyclization by protonating a terminal double bond [5, 6]. The cavity is connected by a nonpolar channel to a hydrophobic plateau structure, which is probably inserted into the nonpolar interior of the membrane (Figure 2). The channel is constricted by residues Phe166, Val174, Phe434, and Cys435

Upon protonation, ring A and probably also ring B are formed in a concerted process [7]. Rings C and D are considered to arise from rearrangements of five-membered rings that were formed by Markovnikov-like ring closure reactions [8, 9]. After cyclization of ring E, the final carbocation on C_{22} is either deprotonated or quenched by a water molecule to yield hopene or diplopterol, respectively (Figure 1B). The carbocationic intermediates are stabilized by cation-π interactions with tryptophans and phenylalanines, which provide an electron-rich but also non-nucleophilic environment [10].

An elevated cholesterol level in the plasma is a major risk factor in the development of atherosclerotic vascular diseases. Currently, cholesterol biosynthesis is reduced by inhibiting the rate-limiting enzyme 3-hydroxy-3-methylglutaryl coenzyme A (HMG-CoA) reductase by so-called statins. These, however, can cause adverse effects due possibly to the suppression of ubiquinone, dolichol, and isopentenyl-tRNA farther along the mevalonate pathway [11]. Moreover, HMG-CoA reductase biosynthesis is upregulated upon inhibition [12]. OSC is an attractive target for novel anticholesteremic drugs because it acts downstream from important branching points in the cholesterol pathway and because the inhibition of OSC happens to avoid accumulation of steroidal intermediates. OSC inhibition raises the concentrations of 2,3;22,23-dioxidosqualene and oxysterols that down-regulate the HMG-CoA reductase activity via a negative-feedback loop.

Potent, orally active inhibitors of human hepatic OSC are Ro48-8071 containing a benzophenone (BP) moiety (Figure 1C) [13], BIBX-79 [14], BIBB-515 [15], and quinuclidine inhibitors [16]. Ro48-8071 inhibited OSC in vitro with an IC_{50} of 6.5 nM for human liver microsomes [13] and 40 nM for homogenous rat liver OSC [17]. Moreover, Ro48-8071 blocked cholesterol biosynthesis in vivo by selective inhibition of OSC in HepG2 cells and, when administered orally, in Syrian hamsters, squirrel monkeys, and Göttingen minipigs [13]. Furthermore, Ro48-8071 was shown to inhibit the SHC from *A. acidocaldarius* [17, 18]. Here we report at 2.8 Å resolution the crystal structure of the SHC:Ro48-8071 complex, showing a binding mode of Ro48-8071 that agrees with the expected binding mode of squalene but differs substantially from a previous model based on photolabeling [18].

Results and Discussion

Kinetic Characterization

The inhibition of the SHC from *A. acidocaldarius* by Ro48-8071 showed an IC_{50} value of 9.0 nM [17]. Moreover, the inhibition pattern suggested noncompetitive

[1]Correspondence: schulz@bio.chemie.uni-freiburg.de

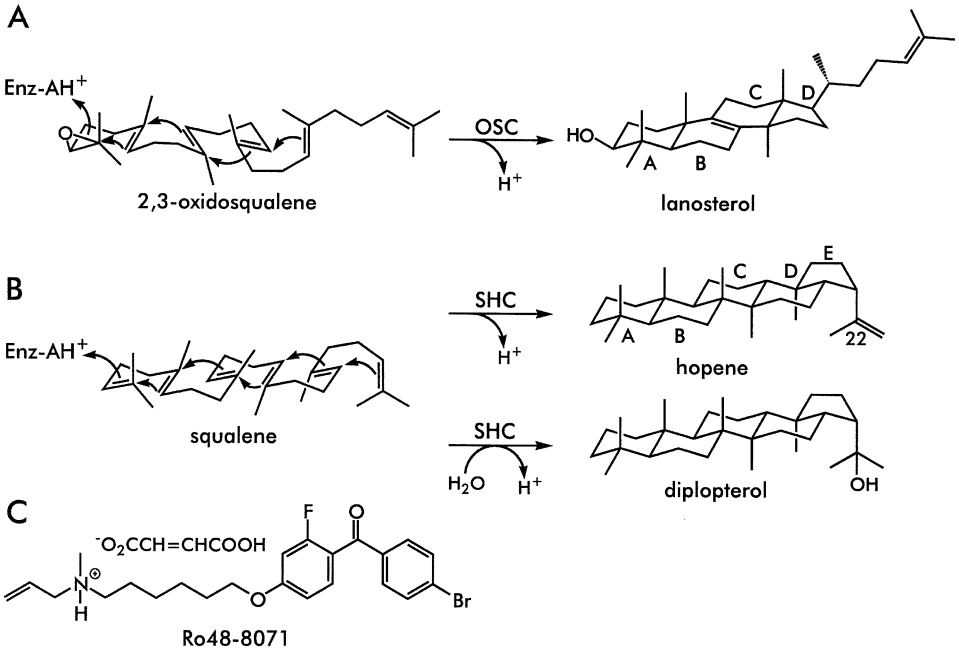

Figure 1. Cyclase Reactions and the Inhibitor Ro48-8071

(A) OSC catalysis.

(B) SHC catalysis.

(C) Inhibitor structure.

action of the compound, implying that the inhibitor site differs from that of the substrate squalene [18]. We repeated the kinetic measurements with an alternative assay, utilizing a gas chromatographic analysis of substrate and product concentrations. For determining the IC_{50} value, the reaction rates were measured at a constant squalene concentration of 20 μM and Ro48-8071 concentrations ranging between 5 nM and 100 μM. The resulting plot showed an IC_{50} value of 61 nM (Figure 3A).

The kinetic properties of SHC were determined with substrate concentrations between 10 μM and 100 μM and Ro48-8071 concentrations up to 60 nM. The resulting double-reciprocal plot showed apparent kinetic constants of k_{cat} = 72 min^{-1} and K_M = 38 μM and a mixed noncompetitive inhibition pattern (Figure 3B). The observed IC_{50}, k_{cat}, and K_M values differ appreciably from previous reports (IC_{50} = 9 nM, k_{cat} = 2.4 min^{-1}, K_M = 1.6 μM in [17]; k_{cat} = 289 min^{-1}, K_M = 16.7 μM in [19]). These variations are most probably caused by different assay methods and different detergents.

Structure of the SHC:Ro48-8071 Complex

The rather nonpolar Ro48-8071 was bound to the dissolved enzyme and subsequently cocrystallized. An initial ($F_{obs} - F_{calc}$)-electron density map was calculated from a 2.8 Å data set collected from three crystals (Table 1). It allowed the unambiguous identification of the inhibitor binding site (Figures 2, 4, and 5). Besides the allyl group, Ro48-8071 was completely outlined at the 3 σ contour level, and the bromo substituent reached a peak height of 11 σ.

The refinement revealed two inhibitor conformations related by a 180° rotation of the fluorophenyl group. The conformation sketched in Figure 1C was the major one, with 62% occupancy. In both conformations fluorine makes comfortable contacts to the environment, namely to Met42-Cε (4.3 Å), Pro263-Cγ (3.5 Å), and Phe605-Cζ (3.6 Å) in the major conformation as well as to Trp169-Cβ (3.1 Å), Trp169-Cδ1 (3.2 Å), and Phe601-Cζ (3.4 Å) in the other. Accordingly, the affinity of the inhibitor may increase upon the introduction of a second fluoro substituent in meta position to the first one.

Ro48-8071 was bound in the large active-center cavity of all three NCS-related protomers in the crystal. It extended from the initial protonation site at the "top" of the cavity down into the putative substrate uptake channel (Figures 2 and 4) occupying 445 $Å^3$ of the 1070 $Å^3$ cavity volume. Several water molecules known from the high-resolution structure [5] had been displaced. The NCS-related protomers showed an rmsd-Cα smaller than 0.2 Å. Moreover, the SHC structure remained unchanged upon Ro48-8071 binding (rmsd-Cα 0.27 Å), indicating that the flexible inhibitor had adapted itself to the rigid active center.

The occupation of the putative squalene site by Ro48-8071 seems to contradict the observed mixed noncompetitive inhibition pattern. It is likely that this discrepancy results from the biphasic state needed for the enzyme activity measurements because the assay requires a detergent for solubilizing the enzyme and the substrate. SHC, squalene, and at least part of Ro48-8071 are located in mixed detergent micelles so that substrate and inhibitor availability may influence the kinetic behavior of the system. As a consequence, the common Michaelis-Menten interpretation [20] is not applicable.

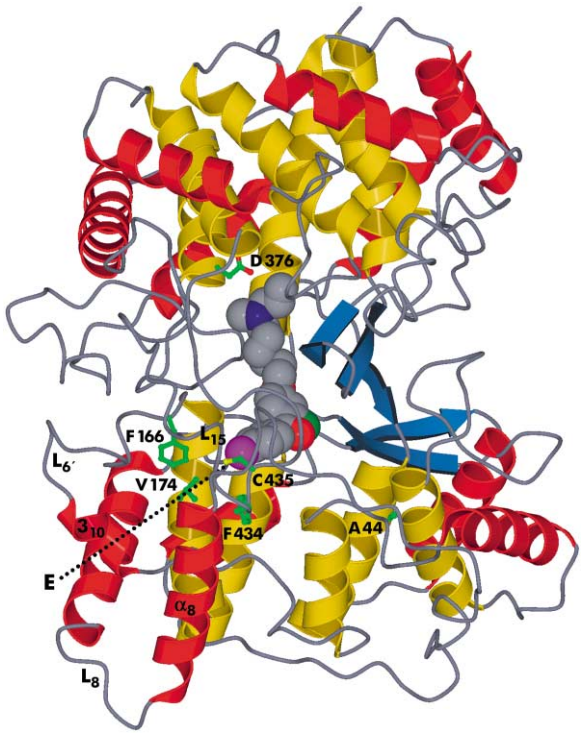

Figure 2. Ribbon Model of SHC with a Space-Filling Model of Bound Ro48-8071

Fluorine is green; bromine is purple. The inner and outer helices are yellow and red, respectively. The channel constriction residues, the putative catalytic acid Asp376 [4], and the photolabeled Ala44 [18] are shown as light-green ball-and-stick models. The nonpolar plateau, assumed to plunge into the nonpolar membrane interior, consists of helices $\alpha 8$ and 3_{10} as well as loops L6′, L8, and L15. It harbors the channel entrance (E), indicated by a dotted line.

Table 1. Data Collection and Refinement Statistics

Space group	$P3_221$
Cell constants (Å)	a = b = 140.9, c = 244.0
Resolution limit (Å)	2.8
Total number of reflections	156′593
Number of unique reflections	54′290
R_{sym}[a,b] (%)	10.0 (20.6)
Completeness[a] (%)	79 (48)
I/σ_1[a]	5.0 (3.4)
Resolution range of refinement[c] (Å)	25–2.8
Number of protein atoms	14′980
Number of water molecules	255
R_{cryst}[b] (%)	20.3
R_{free}[b] (%)	25.9
Average *B* factor, buried atoms (Å^2)	35
Average *B* factor of Ro48-8071 (Å^2)	38

[a] Parentheses refer to the last shells. All data were used without σ cutoff. The threefold NCS averaging may compensate for the low completeness.
[b] $R_{sym} = \Sigma_{hkl,i}|I_{hkl,i} - <I_{hkl}>|/\Sigma_{hkl,i}I_{hkl,i}$; $R_{cryst} = \Sigma_{hkl}||F_{obs}| - k|F_{calc}||/\Sigma_{hkl}|F_{obs}|$; $R_{free} = R_{cryst}$ for a 3.7% test set not used in the refinement.
[c] The rmsd bond lengths and angles were 0.010 Å and 1.46°, respectively. A Ramachandran plot showed 87% of the non-glycine and non-proline residues in the most favored regions and none in the disallowed regions [35]. A *cis*-peptide between Val491 and Asn492 [5] was also present in the complex structure.

Interactions of SHC with Ro48-8071

The alkyl spacer between the benzophenone moiety and the allyl-amino group (Figure 1C) adopts a rather elongated conformation with an N to (ether-)O distance of 7.5 Å (Figure 5). The allyl-amino group is protonated under enzyme assay and crystallization conditions (predicted pK_a, 10.2). It interacts with the amino acid residues that initiate the cyclization and stabilize the early high-energy intermediates (Figure 6). In detail, the protonated amino nitrogen is at a 4.6 Å distance to Asp376-Oδ2 of the conserved sequence motif DXDD and at a 2.9 Å distance to a water molecule known from the high-resolution SHC structure [5]. Moreover, it forms an ion pair with the DXDD motif couple Asp374/Asp377, which probably carries one negative charge [5], and it receives dielectric stabilization from Tyr420 and Tyr609 at hydroxyl oxygen distances of 5.1 and 4.6 Å, respectively. In addition, the protonated amino group is stabilized by cation-π interactions with Trp489, Trp312, and Phe365 at distances between 4.8 and 5.6 Å to the ring centroids. In agreement with ab initio molecular orbital calculations

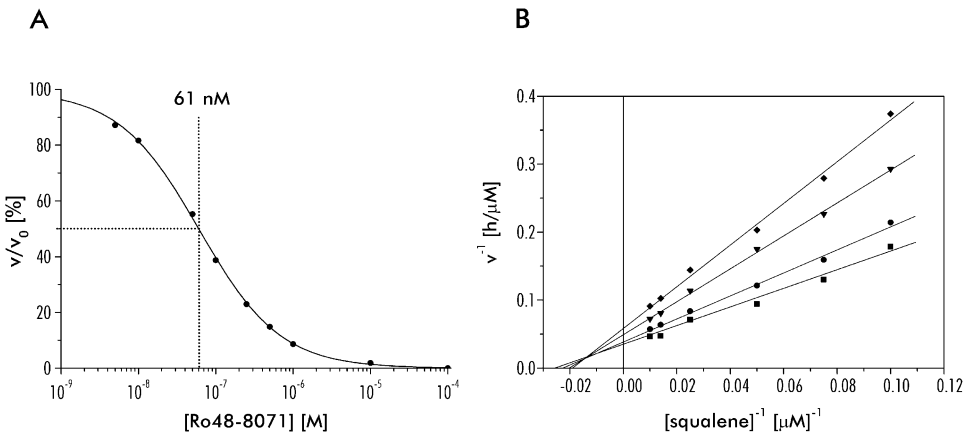

Figure 3. Kinetics of SHC Inhibition by Ro48-8071

(A) Dose-response plot at a squalene concentration of 20 μM.
(B) Double-reciprocal plots for the inhibitor concentrations 0 (squares), 15 (circles), 45 (triangles), and 60 nM (diamonds), respectively.

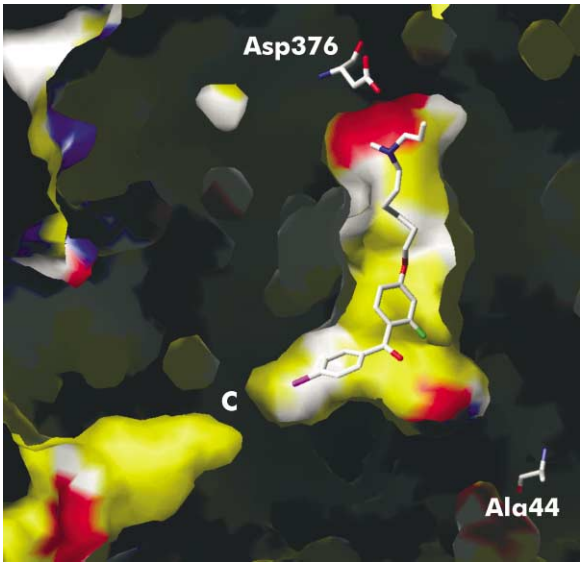

Figure 4. Surface Representation of SHC Sliced through the Middle of the Molecule

The surfaces are colored as nonpolar (yellow) and positively (blue) and negatively (red) charged. The large internal cavity is connected by a nonpolar channel to a hydrophobic surface patch that dips into the membrane. The channel constriction (C) permits substrate passage because Phe434 and Cys435 are on a mobile loop. Ro48-8071 (major conformation) occupies the active-center cavity and the channel up to the constriction. Asp376 and Ala44 are shown as ball-and-stick models.

[21], the ammonium charge is closer to the benzene than to the pyrrol moieties of both tryptophans.

The binding mode of Ro48-8071 resembles that of the detergent N,N-dimethyl-laurylaminoxide (LDAO) found in the first reported crystal structure of SHC [4]. The protonated amino group in conjunction with the hydrogen bonded water molecule is positioned at almost the same site and in almost the same orientation as the aminoxide (Figure 7). Therefore, an optimization of Ro48-8071 directed at mimicking this water position should improve binding. Similar protein-inhibitor interactions have been observed in complexes of acetylcholinesterase with inhibitors containing quaternary ammonium groups [22, 23] (Figure 6). In the so-called "anionic" and "peripheral anionic" subsites of this enzyme, the positive charge is stabilized by cation-π interactions with tryptophans and phenylalanines and by dipoles of tyrosines. A carboxyl oxygen of the anionic subsite was found at a distance of 4.4 Å to the inhibitor nitrogen; this distance matches that observed in the Ro48-8071 complex.

The BP moiety of Ro48-8071 extends into the putative substrate uptake channel (Figures 4 and 5). Phe129 stabilizes the bromophenyl group by an edge-to-face interaction. The observed ring centroid distance is 5.5 Å and corresponds to the most frequent distance of 5.6 Å found for such interactions [24]. The orientation of the Trp169 edge toward the plane of the bromophenyl group with a distance of 5.6 Å between the ring centroids may also indicate a CH-π interaction, although Trp-Phe pairs seem to prefer the reverse geometry [25]. The carbonyl group of the BP moiety lacks a hydrogen bonding partner. This agrees with inhibition studies of OSC in which the inhibitory potency of compounds containing aryl-X-aryl groups [16] shows no dependence on the hydrogen bond acceptor properties of the linker X. In our structure the carbonyl carbon of BP may be stabilized by the π system of Phe605, the centroid of which is located at a distance of 5.3 Å. Because aromatic CH-π interactions are rather weak [24, 26], we suggest that the decisive contribution to the Ro48-8071 position comes from the protonated amino group, in agreement with the almost identical nitrogen position of LDAO (Figure 7).

Comparison with Previous Models

The benzophenone system of tritiated Ro48-8071 was used to photolabel rat liver OSC and *A. acidocaldarius* SHC [17]. The putative attachment site Ala44 of SHC was determined by digestion of labeled protein and subsequent RP-HPLC separation and Edman degradation of the resulting peptides [18]. Consequently, Ala44 was set as a pivotal point in modeling the Ro48-8071:SHC complex. Two inhibitor binding modes, both with the carbonyl oxygen of the BP moiety forming a hydrogen bond with the main chain amide at position 45, were proposed. Both models are distinctly different from the observed binding mode in the crystal, although the inhibitor binding procedures were performed under similar conditions. In our structure the carbonyl carbon of Ro48-8071 and Ala44-C_α are 14 Å apart (Figure 5), which exceeds by far the maximum distance for the photoinduced labeling reaction of 3.1 Å [27]. Moreover, placing Ro48-8071 close to Ala44 requires substantial changes

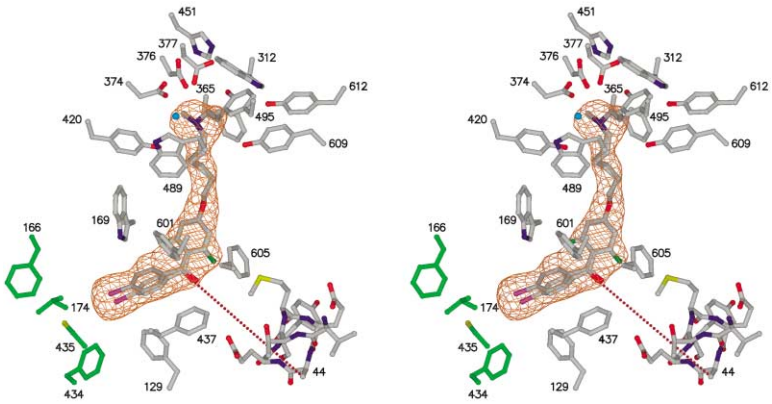

Figure 5. Stereo View of the Binding Mode of Ro48-8071 at SHC

The inhibitor is outlined by an ($F_{obs} - F_{calc}$) omit map of the final model at a contour level of 5 σ. Residues interacting with the inhibitor and residues of the helix containing Ala44 are shown. The four channel constriction residues are in green. The dotted line indicates the 14 Å distance between the carbonyl group of the inhibitor and the photoaffinity-labeled Ala44.

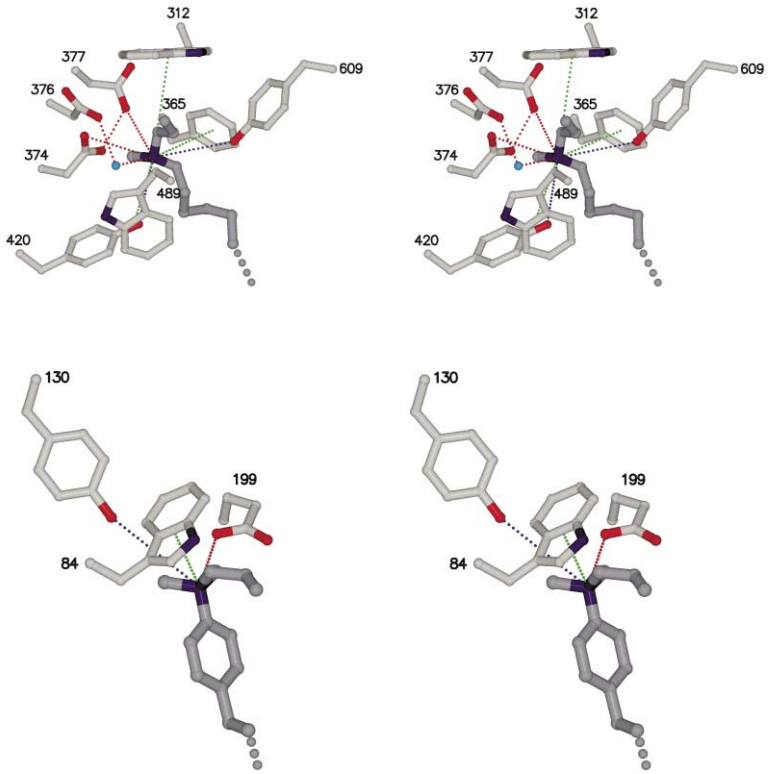

Figure 6. Comparison of Inhibitor Binding in SHC and Acetylcholine Esterase

Stereo view showing the stabilization of the protonated allyl-amino group of Ro48-8071 in SHC (top) and of the quaternary allyl-ammonium group of Bw284C51 at the anionic subsite of acetylcholine esterase (bottom, PDB code 1E3Q). Inhibitor truncations are indicated by large dots. Dotted lines mark cation-π interactions (green), hydrogen bonds, or ion-pair (red) and dipole interactions (blue).

in a rigid part of the protein structure because Ala44 is on that side of an α helix that is turned away from the active-center cavity and therefore not accessible (Figures 4 and 5). Therefore, we conclude that the binding modes derived from photolabeling can be quite different from those in the low-energy crystal structures, possibly because the photolabel may trap the protein in an energetically elevated conformation.

Comparison with Putative Product Binding

Inhibition studies with OSC and compounds similar to Ro48-8071 demonstrated that the distance between the amine nitrogen and the carbonyl carbon influences the inhibitory potency [28]. The lowest IC_{50} values were observed at 10.7 Å, which is approximately the expected distance between the epoxide oxygen and the carbocation position of the protosteryl cation. The respective N-to-C=O distance for bound Ro48-8071 is 12.5 Å, which is slightly larger than the 11.2 Å distance between the initial and final carbocations in hopene (Figures 1B and 7). The hexacarbon spacer of Ro48-8071 adopts a quite elongated conformation so that the C=O group is positioned in an electron-rich environment in the lower part of the active-center cavity. In comparison with the hopene model [5], however, the carbonyl carbon is separated by 2.5 Å from the final carbocation position (Figures 1B and 7). On the other hand, it should be noted that during the cyclization process the hopene scaffold may be shifted along the main axis of the cavity so that the final carbocation position may move farther away from the initiation site.

Significance

Eukaryotic 2,3-oxidosqualene cyclase (OSC) catalyzes a key step in cholesterol biosynthesis. Squalene-

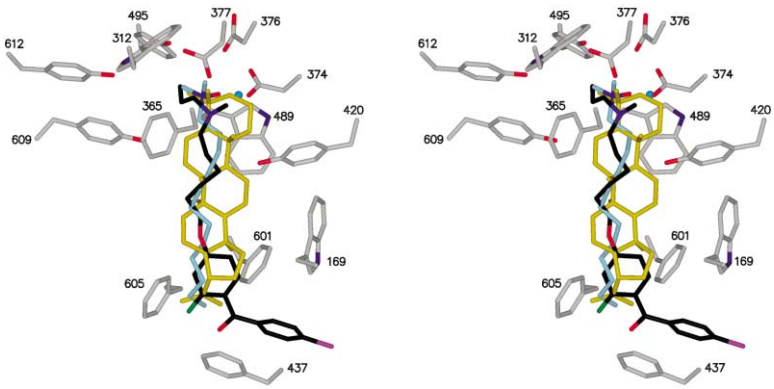

Figure 7. Superposition of Ro48-8071, a Modeled Hopene Molecule, and the Detergent LDAO as Bound to SHC

For clarity, the orientation is rotated by 180° around a vertical axis with respect to the usual view (Figure 5). Hopene [5] is in yellow; LDAO [4] is in light blue. The conformations of the depicted side chains are nearly identical in all established structures, indicating a rigid active center.

hopene cyclase (SHC) is the prokaryotic homolog of OSC, so that the crystal structure of SHC:inhibitor complexes elucidates the interactions determining inhibitor efficiency. The structure of SHC ligated with Ro48-8071, the most potent inhibitor known for this enzyme, was established by X-ray diffraction analysis of cocrystals. Ro48-8071 and, in particular, its bromo substituent were unambiguously identified at the putative squalene binding site in the active center. Its location differs from that of a model based on photoaffinity labeling. The inhibitor position appears to be dominated by the interactions of its protonated amino group, with the amino acid residues catalyzing the protonation of squalene. Further stabilization is achieved by cation and CH-π interactions. The addition of a second fluorine atom and the mimicking of a water molecule hydrogen bonded to the protonated amino group have been proposed as possibilities for future inhibitor development. The apparent discrepancy between the kinetic mixed noncompetitive inhibition pattern and the occupation of the squalene binding site is spurious because the required biphasic system of the assay probably fails to obey Michaelis-Menten kinetics.

Experimental Procedures

Production of SHC:Ro48-8071 Crystals

Recombinant SHC was expressed and purified as previously described [29]. Ro48-8071 was synthesized as described [13]. Purified SHC was dialyzed overnight against 0.6% (w/v) octyltetraoxyethylene (C_8E_4) in Milli-Q water. The protein was incubated at 55°C for 15 min with a 1.5 molar excess of the inhibitor Ro48-8071 in a solution containing 0.6% (w/v) C_8E_4 and 5 mM Tris-HCl (pH 8.0). Crystals were grown in hanging drops containing 5–8 mg/ml SHC, a 1.5 molar excess of the inhibitor, 0.3% (w/v) C_8E_4, 50 mM NaCl, 50 mM sodium citrate (pH 4.8) and 3%–8% (v/v) PEG-600. Crystals of triangular shape and maximum dimensions of about $1000 \times 1000 \times 300$ μm^3 appeared within 1–8 weeks. The established conditions [4] were modified by adding PEG-600 and NaCl in order to grow suitable crystals. The tetragonal crystal form B with superior X-ray diffraction properties [5] could not be obtained.

Kinetic Studies

A published assay was modified [6] for the inhibition kinetics. For the IC_{50} determination of Ro48-8071 (fumarate salt), the reaction mixture contained in a final volume of 1 ml 20 μM squalene, 100 mM sodium citrate (pH 6.0), 0.2% (w/v) taurodeoxycholate, 0.5 μg purified SHC, and one of the following inhibitor concentrations: 5, 10, 50, 100, 250, 500, 1000, 10,000, or 100,000 nM. The mixtures were incubated for 30 min at 60°C, and the reactions were stopped by extraction of the products and the remaining substrate with 2 ml n-hexane/propane-2-ol (3:2, v/v). Squalene, hopene, and diplopterol were identified and quantified with capillary gas chromatography on a DB-1 column (0.32 mm $\times$ 20 m, J & W) in a Vega Series 6000 (Carlo Erba) with the following temperature program: 1 min isothermal at 273°C, 9°C/min in the range 273°C–315°C, and 4 min isothermal at 315°C. Peak areas were integrated with the program CP-Maitre-Elite (version 3.1, Chrompack). The data were analyzed with the fitting function $y = A_2 + (A_1 - A_2)/(1 + (x/IC_{50})^p)$ in the program Origin (version 6.0, Microcal), where y is the residual velocity for the SHC reaction, A_1 and A_2 are the upper and lower asymptotes, x is the Ro48-8071 concentration, and p is the resulting power of the best fit.

The inhibition pattern of Ro48-8071 was determined with the same assay by the use of inhibitor concentrations of 0, 15, 45, and 60 nM and substrate concentrations of 10, 13.3, 20, 40, 70, and 100 μM. The inhibition pattern and the kinetic parameters k_{cat} and K_M were derived from a double-reciprocal plot.

X-Ray Diffraction Analysis

Data to 2.8 Å resolution were collected at room temperature from three isomorphous crystals by the use of an area detector (model X-1000, Nicolet-Bruker) with Cu K_α radiation (model RU200B, Rigaku). Despite an intensive search, we failed to establish a cryo protocol that sufficiently preserved the diffraction quality of the crystals at 100 K. Data were processed with programs XDS [30], SCALA, and TRUNCATE [31]. After rigid body refinement with NCS constraints and the maximum likelihood target in program CNS [32], a $(F_{obs} - F_{calc})$ difference electron density map was calculated by using the SHC structure with water molecules removed as the reference (PDB code 3SQC). Coordinates for an energy-minimized conformation of the inhibitor were generated with the program SYBYL (Tripos, St. Louis/USA), and topology and parameter files were generated with the program XPLO2D [33]. Structural refinement, including all data, bulk solvent correction, and NCS restraints, was performed with the program CNS. Manual rebuilding was done in the program O [34]. *B* factors were refined in groups, with two *B* factors per amino acid (main chain, side chain) and four *B* factors for the inhibitor molecules (amino headgroup, alkyl spacer region, fluorophenyl group, and carbonyl/bromophenyl group). After two alternate conformations of the inhibitor appeared, these were refined with different occupancies because equal occupancies led to unrealistically low *B* factors for one of the conformers. The model quality was assessed with the programs PROCHECK [35] and WHATCHECK [36]. Molecular volumes were calculated with VOIDOO [37] and GRASP [38]. Figures were produced with the programs MOLSCRIPT [39] and Raster3D [40].

Acknowledgments

We thank K. Poralla for the original clone of the SHC from *A. acidocaldarius*, D. Reinert for help with crystallization, and J.D. Aebi, D. Bur, and H. Prinzbach as well as A. Ruf for helpful discussions. This project was supported by the Deutsche Forschungsgemeinschaft under SFB-388.

Received: January 11, 2002
Revised: March 26, 2002
Accepted: April 9, 2002

References

1. Abe, I., Rohmer, M., and Prestwich, G.D. (1993). Enzymatic cyclization of squalene and oxidosqualene to sterols and triterpenes. Chem. Rev. *93*, 2189–2206.
2. Wendt, K.U., Schulz, G.E., Corey, E.J., and Liu, D.R. (2000). Enzyme mechanisms for polycyclic triterpene formation. Angew. Chem. Int. Ed. *39*, 2812–2833.
3. Ourisson, G., and Rohmer, M. (1992). Hopanoids. 2. Biohopanoids: a novel class of bacterial lipids. Acc. Chem. Res. *25*, 403–408.
4. Wendt, K.U., Poralla, K., and Schulz, G.E. (1997). Structure and function of a squalene cyclase. Science *277*, 1811–1815.
5. Wendt, K.U., Lenhart, A., and Schulz, G.E. (1999). The structure of the membrane protein squalene-hopene cyclase at 2.0 Å resolution. J. Mol. Biol. *286*, 175–187.
6. Feil, C., Süssmuth, R., Jung, G., and Poralla, K. (1996). Site-directed mutagenesis of putative active-site residues in squalene-hopene cyclase. Eur. J. Biochem. *242*, 51–55.
7. Jenson, C., and Jorgensen, W.L. (1997). Computational investigations of carbenium ion reactions relevant to sterol biosynthesis. J. Am. Chem. Soc. *119*, 10846–10854.
8. Pale-Grosdemange, C., Feil, C., Rohmer, M., and Poralla, K. (1998). Occurrence of cationic intermediates and deficient control during the enzymatic cyclization of squalene to hopanoids. Angew. Chem. Int. Ed. *37*, 2237–2240.
9. Hoshino, T., Kouda, M., Abe, T., and Ohashi, S. (1999). New cyclization mechanism for squalene: a ring-expansion step for the five-membered C-ring intermediate in hopene biosynthesis. Biosci. Biotechnol. Biochem. *63*, 2038–2041.
10. Dougherty, D.A. (1996). Cation-π interactions in chemistry and biology: a new view of benzene, Phe, Tyr, and Trp. Science *271*, 163–168.

11. Grünler, J., Ericsson, J., and Dallner, G. (1994). Branch-point reactions in the biosynthesis of cholesterol, dolichol, ubiquinone and prenylated proteins. Biochim. Biophys. Acta *1212*, 259–277.
12. Qin, W., Infante, J., Wang, S.R., and Infante, R. (1992). Regulation of HMG-CoA reductase, apoprotein-B and LDL receptor gene expression by the hypocholesterolemic drugs simvastatin and ciprofibrate in Hep G2, human and rat hepatocytes. Biochim. Biophys. Acta *1127*, 57–66.
13. Morand, O.H., Aebi, J.D., Dehmlow, H., Ji, Y.H., Gains, N., Lengsfeld, H., and Himber, J. (1997). Ro48–8071, a new 2,3-oxidosqualene:lanosterol cyclase inhibitor lowering plasma cholesterol in hamsters, squirrel monkeys, and minipigs: comparison to simvastatin. J. Lipid Res. *38*, 373–390.
14. Mark, M., Müller, P., Maier, R., and Eisele, B. (1996). Effects of a novel 2,3-oxidosqualene cyclase inhibitor on the regulation of cholesterol biosynthesis in HepG2 cells. J. Lipid Res. *37*, 148–158.
15. Eisele, B., Budzinski, R., Müller, P., Maier, R., and Mark, M. (1997). Effects of a novel 2,3-oxidosqualene cyclase inhibitor on cholesterol biosynthesis and lipid metabolism in vivo. J. Lipid Res. *38*, 564–575.
16. Brown, G.R., Hollinshead, D.M., Stokes, E.S.E., Clarke, D.S., Eakin, M.A., Foubister, A.J., Glossup, S.C., Griffiths, D., Johnson, M.C., and McTaggart, F. (1999). Quinuclidine inhibitors of 2,3-oxidosqualene cyclase-lanosterol synthase: optimization from lipid profiles. J. Med. Chem. *42*, 1306–1311.
17. Abe, I., Zheng, Y.F., and Prestwich, G.D. (1998). Photoaffinity labeling of oxidosqualene cyclase and squalene cyclase by a benzophenone-containing inhibitor. Biochemistry *37*, 5779–5784.
18. Dang, T., Abe, I., Zheng, Y.F., and Prestwich, G.D. (1999). The binding site for an inhibitor of squalene:hopene cyclase determined using photoaffinity labeling and molecular modeling. Chem. Biol. *6*, 333–341.
19. Sato, T., and Hoshino, T. (1999). Functional analysis of the DXDDTA motif in squalene-hopene cyclase by site-directed mutagenesis experiments: initiation site of the polycyclization reaction and stabilization site of the carbocation intermediate of the initially cyclized A-ring. Biosci. Biotechnol. Biochem. *63*, 2189–2198.
20. Bisswanger, H. (2000). Enzymkinetik. (Weinheim, Germany: Wiley-VCH), pp 90–91.
21. Mecozzi, S., West, A.P., Jr., and Dougherty, D.A. (1996). Cation-π interactions in aromatics of biological and medicinal interest: electrostatic potential surfaces as a useful qualitative guide. Proc. Natl. Acad. Sci. USA *93*, 10566–10571.
22. Harel, M., Schalk, I., Ehret-Sabatier, L., Bouet, F., Goeldner, M., Hirth, C., Axelsen, P.H., Silman, I., and Sussman, J.L. (1993). Quaternary ligand binding to aromatic residues in the active-site gorge of acetylcholinesterase. Proc. Natl. Acad. Sci. USA *90*, 9031–9035.
23. Doucet-Personeni, C., Bentley, P.D., Fletcher, R.J., Kinkaid, A., Kryger, G., Pirard, B., Taylor, A., Taylor, R., Taylor, J., Viner, R., et al. (2001). A structure-based design approach to the development of novel, reversible AChE inhibitors. J. Med. Chem. *44*, 3203–3215.
24. Burley, S.K., and Petsko, G.A. (1985). Aromatic-aromatic interaction: a mechanism of protein structure stabilization. Science *229*, 23–28.
25. Samanta, U., Pal, D., and Chakrabarti, P. (1999). Packing of aromatic rings against tryptophan residues in proteins. Acta Crystallog. D *55*, 1421–1427.
26. Adams, H., Carver, F., Hunter, C.A., Morales, J., and Seward, E.M. (1996). Chemical double-mutant cycles for the measurement of weak intermolecular interactions—edge-to-face aromatic interactions. Angew. Chem. Int. Ed. Engl. *35*, 1542–1544.
27. Dormán, G., and Prestwich, G.D. (1994). Benzophenone photophores in biochemistry. Biochemistry *33*, 5661–5673.
28. Jolidon, S., Polak-Wyss, A., Hartman, P.G., and Guerry, P. (1993). 2,3-Oxidosqualene-lanosterol cyclase: an attractive target for antifungal drug design. In Recent Advances in the Chemistry of Anti-infective Agents, P.H. Bentley, ed. (Cambridge, UK: Royal Soc. Chemistry), pp 223–233.
29. Wendt, K.U., Feil, C., Lenhart, A., Poralla, K., and Schulz, G.E. (1997). Crystallization and preliminary X-ray crystallographic analysis of squalene-hopene cyclase from *Alicyclobacillus acidocaldarius*. Protein Sci. *6*, 722–724.
30. Kabsch, W. (1998). Evaluation of single-crystal X-ray diffraction from a position-sensitive detector. J. Appl. Crystallogr. *21*, 916–924.
31. CCP4 (Collaborative Computational Project 4) (1994). The CCP4 suite: programs for protein crystallography. Acta Crystallogr. D *50*, 760–763.
32. Brünger, A.T., Adams, P.D., Clore, G.M., DeLano, W.L., Gros, P., Grosse-Kunstleve, R.W., Jiang, J.S., Kuszewski, J., Nilges, M., Pannu, N.S., et al. (1998). Crystallography and NMR system: a new software suite for macromolecular structure determination. Acta Crystallogr. D *54*, 905–921.
33. Kleywegt, G.J. (1995). Dictionaries for Heteros. CCP4/ESF-EACBM Newsletter on Protein Crystallography *31*, pp 45–50.
34. Jones, T.A., Zou, J.Y., Cowan, S.W., and Kjeldgaard, M. (1991). Improved methods for building protein models in electron-density maps and the location of errors in these models. Acta Crystallogr. A *47*, 110–119.
35. Laskowski, R.A., MacArthur, M.W., Moss, D.S., and Thornton, J.M. (1993). PROCHECK: a program to check the stereochemical quality of protein structures. J. Appl. Crystallogr. *26*, 283–291.
36. Hooft, R.W.W., Vriend, G., Sander, C., and Abola, E.E. (1996). Errors in protein structures. Nature *381*, 272.
37. Kleywegt, G.J., and Jones, T.A. (1994). Detection, delineation, measurement and display of cavities in macromolecular structures. Acta Crystallogr. D *50*, 178–185.
38. Nicholls, A., Sharp, K.A., and Honig, B. (1991). Protein folding and association: insight from the interfacial and thermodynamic properties of hydrocarbons. Proteins: Struct. Funct. Genet. *11*, 281–296.
39. Kraulis, P.J. (1991). MOLSCRIPT—a program to produce both detailed and schematic plots of protein structures. J. Appl. Crystallogr. *24*, 946–950.
40. Merritt, E.A., and Bacon, D.J. (1997). Raster3D: photorealistic molecular graphics. Methods Enzymol. *277*, 505–524.

Accession Numbers

The coordinates and structure factors are deposited in the Protein Data Bank under accession code 1GSZ.